IMPACTS OF HETEROGENOUS-HOMOGENEOUS REACTIONS IN THE FLOW OF PRANDTL NANOFLUIDS WITH CONVECTIVE HEATING PROCESS

by

Mohammed A. ALGHAMDI and Malik Zaka ULLAH*

Department of Mathematics, Faculty of Science, King Abdulaziz University, Jeddah, Saudi Arabia

Original scientific paper
https://doi.org/10.2298/TSCI21S2387A

This research article discusses the 3-D flow of magnetized Prandtl nanoliquid by convectively heated surface utilizing homogeneous-heterogeneous reactions. An extendable surface produces the flow. Thermophoresis and random development are investigated. Thermal transport for the convective method is accounted. The Prandtl material is an electrical conducting via applying a magnetic field. Appropriate non-dimensional factors correspond to the non-linear differential equations. Acquired non-linear differential frameworks are comprehended via the optimal homotopic procedure. Physical amounts like surface drag force and rate of the heat transfer are investigated through sketches. It is seen that the impacts of Biot and Hartman numbers on the concentration and the temperature are very comparative. Both the concentration and the temperature are improved for growing estimations of Biot and Hartman numbers.

Key words: *3-D flow, Prandtl fluid, MHD, convective heating process, nanoparticles, heterogeneous-homogeneous reactions*

Introduction

The nanofluid phenomenon is an interesting topic for scientists and researchers because of its many practical significance in modern nanotechnology and manufacturing. Nanofluids play a significant role in thermal energy tools as an excellent unusual for improving the performance of mass and heat transport apparatus and reducing the mass of the device, and generating electricity. To progress the effectiveness of flat plate solar collectors, scholars performed observational and methodological research projects on smooth plate solar thermal utilizing nanofluids with specific binary components (nanofluids) as operating fluids. Because the water is a good reference point for convection and is also an excellent medium for collecting and storing solar energy during the sunrise, thus water is a suitable medium for heating activities and a significant source for solar energy use. Nanofluid mechanism accomplished various wide range applications in modern nanotechnologies, chemical and mechanical industries like paper cooling, crystal growing, vitality, hardware, and microelectronics. Nanoparticles sizing from 1 nm to 100 nm have particular chemical, technological and mechanical characteristics and thus offer unique opportunities to tackle oil production challenges in a novel way. Compared to several other functional nanofluids, magnetic nanoparticles (MNP) have a various wide range

* Corresponding author, e-mail: zmalek@kau.edu.sa

of exclusive magnetic characteristics which give them a significant advantage in underground transport manipulation. Utilizes of MNP for pharmaceutical and biomedical applications is generally classified into two types: implementation in vitro and application in vivo. The vitro involves separation and filtration, magneto faction immunology, and magnetic solid-phase processing, and in vivo implementations include chiefly medical treatments for example, hyperthermia treatment and targeted drug delivery and diagnoses like functional magnetic resonance and mass spectroscopy tomography. Nanofluids were firstly termed by Choi [1]. Then Buongiorno [2] explored relationship to examine the features of Brownian movement and thermophoresis. Few investigations on nanofluids can be represented by examinations [3-15].

Chemical responses are masterminded into heterogeneous-homogeneous responses related to different artificially reacting-structure such as consuming, bio-chemical and catalysis systems. Such reactions react especially in non-attendance or closeness of impulse. In the homogeneous reaction, the driving force works in a similar stage however if there ought to emerge, an event of the heterogeneous-reaction catalyst works in the numerous stage. Usages of mixture responses consolidate sustenance assimilation in body, polymer age, impact of fireworks, collecting of pottery creation, hydrometallurgical gadgets, biochemical structures, refining process and fog course of action. Viscous flow subject to heterogeneous-homogeneous responses is accounted by Merkin [16]. Heterogeneous-homogeneous responses subject to equal diffusivities are inspected by Chaudary and Merkin [17]. Kameswaran *et al.* [18] discussed nanofluid streams through vulnerable surfaces subject to heterogeneous-homogeneous responses. Heterogeneous-homogeneous responses in MHD streams provoked by twisted expanding plate are represented by Imtiaz *et al.* [19]. Heterogeneous-homogeneous responses in the magnetized Fe_3O_4 nanoliquid stream with the radiative surface is analyzed by Sajid *et al.* [20]. Modified Fick's and Fourier's laws for the 3-D stream of visco-elastic liquid were explored by Hayat *et al.* [21]. Khan *et al.* [22] provided viscous liquid Darcy Forchheimer stream with heterogeneous-homogeneous responses.

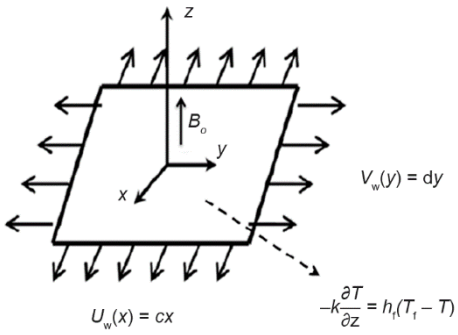

Figure 1. The sketch of the model

The prime reason for the present subject is to outline heterogeneous-homogeneous responses in the magnetized 3-D Prandtl liquid flow [23-26] within sight of the nanomaterials. Mass and thermal exchange properties are depicted via arbitrary motion and thermophoretic diffusion. Thermally convection [27, 28] and flux of zero nanoparticles [29, 30] at the boundary are utilized. Acquired nonlinear differential frameworks are computed via OHAM [31-37]. The impacts of different physical factors are examined. Moreover, the surface drags and heat transport rate is investigated via sketches, fig. 1.

Model development

The steady, 3-D flow of magnetized Prandtl nanoliquid by extendable linear surface with heterogeneous-homogeneous responses is presented. Random movement and thermophoretic features are accounted. The surface is extended along x- and y-axes at $z = 0$ subject to velocities U_w and V_w. The homogeneous-response for the cubic-catalysis is [16, 21]:

$$A + B \rightarrow 3B, \quad \text{rate} = k_c ab^2 \tag{1}$$

At the catalyst-surface, the heterogeneous-response is [16, 21]:

$$A \to B, \quad \text{rate} = k_s a \tag{2}$$

Here k_c, k_s, and A, B are the constants and chemical-species. The flow equations are:

$$\frac{\partial u}{\partial x} + \frac{\partial v}{\partial y} + \frac{\partial w}{\partial z} = 0 \tag{3}$$

$$u\frac{\partial u}{\partial x} + v\frac{\partial u}{\partial y} + w\frac{\partial u}{\partial z} = \nu\frac{A^*}{c^*}\frac{\partial^2 u}{\partial z^2} + \frac{\nu A^*}{2c^{*3}}\left(\frac{\partial u}{\partial z}\right)^2\frac{\partial^2 u}{\partial z^2} - \frac{\sigma B_0^2}{\rho_f}u \tag{4}$$

$$u\frac{\partial v}{\partial x} + v\frac{\partial v}{\partial y} + w\frac{\partial v}{\partial z} = \nu\frac{A^*}{c^*}\frac{\partial^2 v}{\partial z^2} + \frac{\nu A^*}{2c^{*3}}\left(\frac{\partial v}{\partial z}\right)^2\frac{\partial^2 v}{\partial z^2} - \frac{\sigma B_0^2}{\rho_f}v \tag{5}$$

$$u\frac{\partial T}{\partial x} + v\frac{\partial T}{\partial y} + w\frac{\partial T}{\partial z} = \alpha^*\frac{\partial^2 T}{\partial z^2} + \frac{(\rho c)_p}{(\rho c)_f}\left[D_B^*\left(\frac{\partial T}{\partial z}\frac{\partial C}{\partial z}\right) + \frac{D_T}{T_\infty}\left(\frac{\partial T}{\partial z}\right)^2\right] \tag{6}$$

$$u\frac{\partial C}{\partial x} + v\frac{\partial C}{\partial y} + w\frac{\partial C}{\partial z} = D_B^*\left(\frac{\partial^2 C}{\partial z^2}\right) + \frac{D_T}{T_\infty}\left(\frac{\partial^2 T}{\partial z^2}\right) \tag{7}$$

$$u\frac{\partial a}{\partial x} + v\frac{\partial a}{\partial y} + w\frac{\partial a}{\partial z} = D_A\left(\frac{\partial^2 a}{\partial z^2}\right) - k_c a b^2 \tag{8}$$

$$u\frac{\partial b}{\partial x} + v\frac{\partial b}{\partial y} + w\frac{\partial b}{\partial z} = D_B\left(\frac{\partial^2 b}{\partial z^2}\right) + k_c a b^2 \tag{9}$$

$$\begin{gathered} u = U_w = cx, \quad v = V_w = dy, \quad w = 0, \quad -k\frac{\partial T}{\partial z} = h_f(T_f - T) \\ D_B^*\frac{\partial C}{\partial z} + \frac{D_T}{T_\infty}\frac{\partial T}{\partial z} = 0, \quad D_A\frac{\partial a}{\partial z} = k_s a, \quad D_B\frac{\partial b}{\partial z} = -k_s a \quad \text{at} \quad z = 0 \end{gathered} \tag{10}$$

$$u \to 0, \quad v \to 0, \quad T \to T_\infty, \quad C \to C_\infty, \quad a \to a_0, \quad b \to 0 \quad \text{as} \quad z \to \infty \tag{11}$$

where u, v, and w are velocities in x-, y-, and z-axes, respectively, while σ, D_T, and μ denote electrical conductivity, thermophoretic diffusivity, and dynamic viscosity, respectively, A^* and c^* the material constants, ν ($= \mu/\rho_f$) – the kinematic viscosity, $\alpha^* = k/(\rho c)_f$, k, and C – the thermal diffusion, thermal conductivity, and concentration of the nanoparticles, respectively $(\rho c)_f$ – the heat capacity of liquid, ρ_f – the density, and T_∞, C_∞ – the ambient temperature and concentrations. Considering:

$$\begin{gathered} u = cxf'(\zeta), \quad v = cyg'(\zeta), \quad w = -(c\nu)^{1/2}[f(\zeta) + g(\zeta)], \quad \theta(\zeta) = \frac{T - T_\infty}{T_f - T_\infty} \\ \phi(\zeta) = \frac{C - C_\infty}{C_\infty}, \quad \zeta = \left(\frac{c}{\nu}\right)^{1/2} z, \quad a = a_0 r(\zeta), \quad b = a_0 h(\zeta) \end{gathered} \tag{12}$$

Continuity relation (3) is confirmed while eqs. (4)-(11) yield:

$$\beta_1 f''' + (f + \mathrm{g}) f'' - f'^2 + \beta_2 f''^2 f''' - \mathrm{Ha}^2 f' = 0 \tag{13}$$

$$\beta_1 \mathrm{g}''' + (f + \mathrm{g})\mathrm{g}'' - \mathrm{g}'^2 + \beta_2 \mathrm{g}''^2 \mathrm{g}''' - \mathrm{Ha}^2 \mathrm{g}' = 0 \tag{14}$$

$$\theta'' + \mathrm{Pr}[(f + \mathrm{g})\theta' + N_b \theta' \phi' + N_t \theta'^2] = 0 \tag{15}$$

$$\phi'' + \mathrm{Sc}(f + \mathrm{g})\phi' + \frac{N_t}{N_b}\theta'' = 0 \tag{16}$$

$$\frac{1}{\mathrm{Sc}_b} r'' + (f + \mathrm{g}) r' - k_1 r h^2 = 0 \tag{17}$$

$$\frac{\delta}{\mathrm{Sc}_b} h'' + (f + \mathrm{g}) h' + k_1 r h^2 = 0 \tag{18}$$

$$\begin{aligned} &f(0) = \mathrm{g}(0) = 0, \quad f'(0) = 1, \quad \mathrm{g}'(0) = \alpha, \quad \theta'(0) = -\gamma[1 - \theta(0)] \\ &N_b \phi'(0) + N_t \theta'(0) = 0, \quad r'(0) = k_2 r(0), \quad \delta h'(0) = -k_2 r(0) \end{aligned} \tag{19}$$

$$f'(\infty) = \mathrm{g}'(\infty) = \phi(\infty) = h(\infty) = \theta(\infty) \to 0, \quad r(\infty) \to 1 \tag{20}$$

where β_1 and β_2 stand for Prandtl fluid numbers, Ha – the Hartman parameter, Pr – the Prandtl number, α – the ratio factor, γ – the Biot factor, Sc – the Schmidt factor, N_b – the Brownian development factor, N_t – the thermophoresis factor, k_1 – the the strength of homogeneous reaction, Sc_b – the Schmidt number, δ – the the ratio of mass diffusion coefficients, and k_2 – the the strength of the heterogeneous reaction. These pertinent parameters are characterized by:

$$\begin{aligned} &\beta_1 = \frac{1}{\mu A^* c^*}, \quad \beta_2 = \frac{\mathrm{d}U_\mathrm{w}}{2c^{*2}\nu}, \quad \mathrm{Ha}^2 = \frac{\sigma B_0^2}{c\rho_\mathrm{f}}, \quad \alpha = \frac{d}{c}, \quad \gamma = \frac{h_\mathrm{f}}{k}\sqrt{\frac{\nu}{c}} \\ &N_b = \frac{(\rho c)_p D_\mathrm{B}^* C_\infty}{(\rho c)_\mathrm{f} \nu}, \quad N_t = \frac{(\rho c)_p D_\mathrm{T}(T_\mathrm{f} - T_\infty)}{(\rho c)_\mathrm{f} \nu T_\infty}, \quad \mathrm{Pr} = \frac{\nu}{\alpha^*}, \quad \mathrm{Sc} = \frac{\nu}{D_\mathrm{B}^*} \\ &k_1 = \frac{k_\mathrm{c} a_0^2}{U_\mathrm{w}}, \quad k_2 = \frac{k_\mathrm{s}}{D_A a_0}\sqrt{\frac{c}{\nu}}, \quad \delta = \frac{D_\mathrm{B}}{D_A}, \quad Sc_b = \frac{\nu}{D_A} \end{aligned} \tag{21}$$

Assuming that $D_A = D_\mathrm{B}$ we have $\delta = 1$ and thus:

$$r(\zeta) + h(\zeta) = 1 \tag{22}$$

Now eqs. (17) and (18) yield:

$$\frac{1}{Sc_b} r'' + (f + \mathrm{g}) r' - k_1 (1 - r)^2 r = 0 \tag{23}$$

with the boundary conditions:

$$r'(0) = k_2 r(0), \quad r(\infty) \to 1 \tag{24}$$

The physical quantities are given by:

$$\mathrm{Re}_x^{1/2}C_\mathrm{f} = [\beta_1 f''(0) + \beta_2 f''(0)^3], \quad \mathrm{Re}_y^{1/2}C_\mathrm{g} = [\beta_1 \mathrm{g}''(0) + \beta_2 \mathrm{g}''(0)^3], \quad \mathrm{Re}_x^{-1/2}\mathrm{Nu}_x = -\theta'(0) \tag{25}$$

where $\mathrm{Re}_x = U_\mathrm{w}x/\nu$ and $\mathrm{Re}_y = V_\mathrm{w}y/\nu$ stands for local Reynolds numbers. The presented results are converted to Newtonian fluid flow case when $\beta_1 = 1$ and $\beta_2 = 0$.

The OHAM solutions

The manuscript, linear operators, and initial guesses for the homotopic solutions are:

$$\begin{gathered} f_0(\zeta) = 1 - \mathrm{e}^{-\zeta}, \quad \mathrm{g}_0(\zeta) = \alpha(1 - \mathrm{e}^{-\zeta}), \quad \theta_0(\zeta) = \frac{\gamma}{1+\gamma}\mathrm{e}^{-\zeta} \\ \phi_0(\zeta) = -\frac{\gamma}{1+\gamma}\frac{N_t}{N_b}\mathrm{e}^{-\zeta}, \quad r_0(\zeta) = 1 - \frac{1}{2}\mathrm{e}^{-k_2\zeta} \end{gathered} \tag{26}$$

$$\begin{gathered} \mathcal{L}_\mathrm{f} = \frac{\mathrm{d}^3 f}{\mathrm{d}\zeta^3} - \frac{\mathrm{d}f}{\mathrm{d}\zeta}, \quad \mathcal{L}_g = \frac{\mathrm{d}^3 \mathrm{g}}{\mathrm{d}\zeta^3} - \frac{\mathrm{d}\mathrm{g}}{\mathrm{d}\zeta}, \quad \mathcal{L}_\theta = \frac{\mathrm{d}^2\theta}{\mathrm{d}\zeta^2} - \theta \\ \mathcal{L}_\phi = \frac{\mathrm{d}^2\phi}{\mathrm{d}\zeta^2} - \phi, \quad \mathcal{L}_r = \frac{\mathrm{d}^2 r}{\mathrm{d}\zeta^2} - r \end{gathered} \tag{27}$$

The aforementioned linear operators satisfy:

$$\begin{gathered} \mathcal{L}_\mathrm{f}(H_1^{****} + H_2^{****}\mathrm{e}^{\zeta} + H_3^{****}\mathrm{e}^{-\zeta}) = 0, \quad \mathcal{L}_\mathrm{g}(H_4^{****} + H_5^{****}\mathrm{e}^{\zeta} + H_6^{****}\mathrm{e}^{-\zeta}) = 0 \\ \mathcal{L}_\theta[H_7^{****}\mathrm{e}^{\zeta} + H_8^{****}\mathrm{e}^{-\zeta}] = 0, \quad \mathcal{L}_\phi[H_9^{****}\mathrm{e}^{\zeta} + H_{10}^{****}\mathrm{e}^{-\zeta}] = 0 \\ \mathcal{L}_r[H_{11}^{****}\mathrm{e}^{\zeta} + H_{12}^{****}\mathrm{e}^{-\zeta}] = 0.28 \end{gathered} \tag{28}$$

in which H_j^{****} (j = 1-12) indicate constants. The 0$^{\mathrm{th}}$ and m^{th} orders deformations are defined easily *via* the mentioned operators by BVPH 2.0. Figure 2 represents the sum of the square residual-error. Table 1 displays that averaged squared residual error presents a decaying situation with the higher-order deformations.

Table 1. Numerical values of the errors using the optimal data of the auxiliary variables

$\tilde{m}$	$\varepsilon_{\tilde{m}}^{f}$	$\varepsilon_{\tilde{m}}^{g}$	$\varepsilon_{\tilde{m}}^{\theta}$	$\varepsilon_{\tilde{m}}^{\varphi}$	$\varepsilon_{\tilde{m}}^{r}$
2	8.14×10^{-4}	2.91×10^{-5}	4.30×10^{-5}	5.34×10^{-5}	2.16×10^{-4}
6	7.48×10^{-5}	1.62×10^{-6}	5.93×10^{-6}	1.65×10^{-5}	1.25×10^{-4}
10	1.89×10^{-5}	2.23×10^{-7}	2.51×10^{-6}	9.18×10^{-6}	8.50×10^{-5}
16	4.47×10^{-6}	2.97×10^{-8}	1.09×10^{-6}	5.01×10^{-6}	6.11×10^{-5}
20	2.12×10^{-6}	1.25×10^{-8}	7.19×10^{-7}	3.69×10^{-6}	4.85×10^{-5}
24	1.12×10^{-6}	6.43×10^{-9}	5.05×10^{-7}	2.85×10^{-6}	4.27×10^{-5}
30	5.02×10^{-7}	2.92×10^{-9}	3.23×10^{-7}	2.07×10^{-6}	3.25×10^{-5}

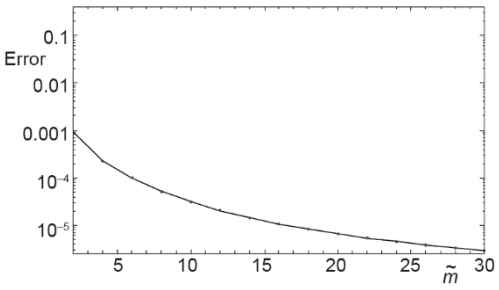

Figure 2. Sketch of total residual – error

Graphical findings and discussion

This portion depicts the features of several emerging flow variables such as Prandtl liquid parameters β_1 and β_2, Hartman number, heterogeneous reaction parameter, k_2, ratio number, α, Biot parameter,γ, Schmidt number, Sc_b (for heterogeneous-homogeneous reactions), Prandtl factor, Schmidt parameter, homogeneous-reaction parameter k_1, Brownian factor, N_b, and thermophoresis factor, N_t, on the temperature, $\theta(\zeta)$, concentration, $\phi(\zeta)$, and concentration rate, $r(\zeta)$. Figures 3 and 4 are displayed to explore temperature, $\theta(\zeta)$, for different data of β_1 and β_2. Here expansion in the β_1 and β_2 prompts a decline in temperature. Figure 5 shows the varieties of Hartman number on temperature profile, $\theta(\zeta)$. Lorentz power emerges in Hartman number that opposes the smooth movement in this manner temperature field, $\theta(\zeta)$, upgrades. Figure 6 exhibits that a change in degree number, α, prompts a helpless temperature, $\theta(\zeta)$. The effect of the Biot factor, γ, on the $\theta(\zeta)$ is delineated in fig. 7. Increment in the γ produces ground-breaking convection that shows augmentation in the $\theta(\zeta)$. Figure 8 displays that $\theta(\zeta)$ reduces for more noteworthy estimations of Prandtl number. As more prominent Prandtl number relates to bringing down warm diffusivity which causes a decline in temperature. Figure 9 is developed to consider impact of N_t on temperature $\theta(\zeta)$. An expansion in N_t keeps an eye on more temperature. Such boundary is happened because of nanomaterials. The presence of the nanomaterials enhanced the warm conductivity. Nanofluid warm conductivity is expanding the capacity of $\theta(\zeta)$. That is the reason upgrade in $\theta(\zeta)$ is watched for more prominent data of N_t. Figures 10 and 11 clarify that concentration is littler for the more prominent estimations of β_1 and β_2 (material boundaries). Figures 12 and 13 are sketched to investigate variation in the $\phi(\zeta)$ for the bigger Hartman number and α. We saw that reverse impacts happen for both Hartman number and α on concentration profiles. Figure 14 displays outcomes of Scmidt number on the $\phi(\zeta)$. The Schmidt factor identifies with the mass dissemination of the framework. As the Scmidt number has been

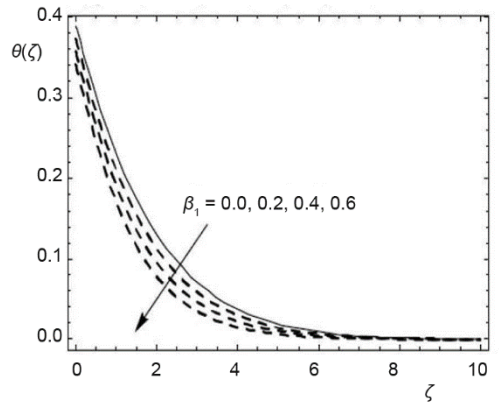

Figure 3. Curves of β_1 contrasted with $\theta(\zeta)$; β_1 = 0.5, Ha = N_t = 0.1, α = γ = N_b = 0.3, Sc = Pr = 1.0

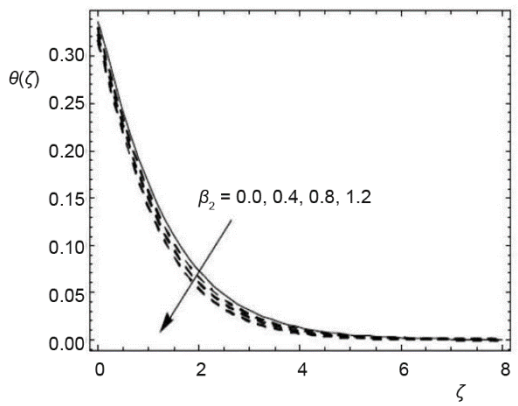

Figure 4. Curves of β_2 contrasted with $\theta(\zeta)$; β_1 = 0.5, Ha = N_t = 0.1, α = γ = N_b = 0.3, Sc = Pr = 1.0

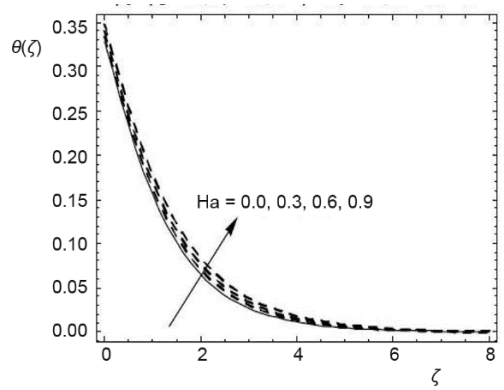

Figure 5. Curves of Hartman number contrasted with $\theta(\zeta)$; $\beta_1 = \beta_2 = 0.5$, $N_t = 0.1$, $\alpha = \gamma = N_b = 0.3$, Sc = Pr = 1.0

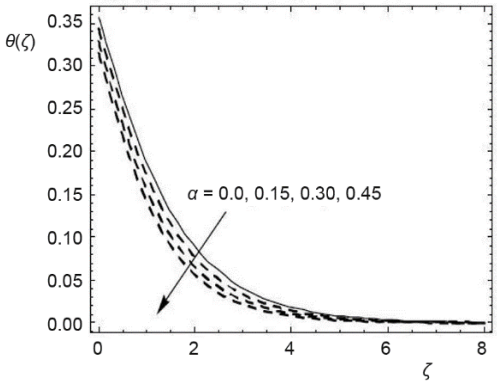

Figure 6. Curves of α contrasted with $\theta(\zeta)$; $\beta_1 = \beta_2 = 0.5$, Ha = $N_t = 0.1$, $\gamma = N_b = 0.3$, Sc = Pr = 1.0

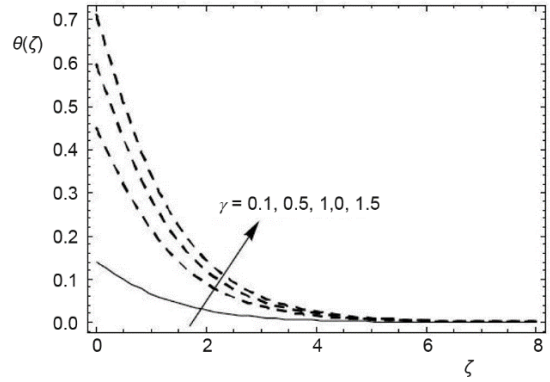

Figure 7. Curves of γ contrasted with $\theta(\zeta)$; $\beta_1 = \beta_2 = 0.5$, Ha = $N_t = 0.1$, $\alpha = N_b = 0.3$, Sc = Pr = 1.0

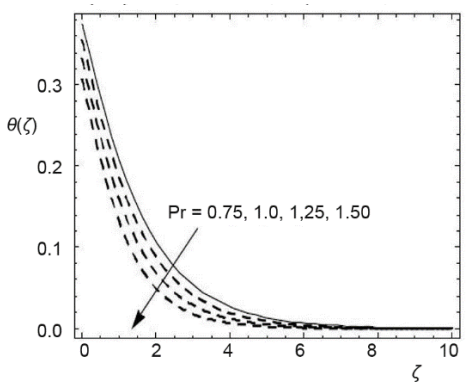

Figure 8. Curves of Prandtl number contrasted with $\theta(\zeta)$; $\beta_1 = \beta_2 = 0.5$, Ha = $N_t = 0.1$, $\alpha = \gamma = N_b = 0.3$, Sc = 1.0

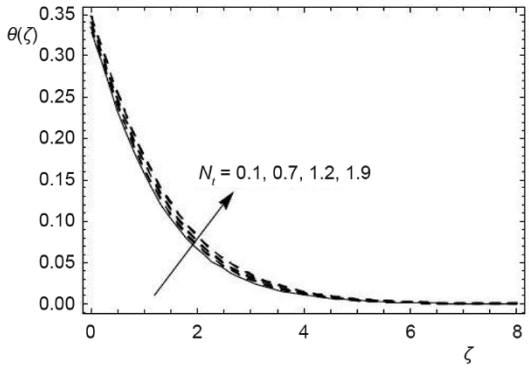

Figure 9. Curves of N_t contrasted with $\theta(\zeta)$; $\beta_1 = \beta_2 = 0.5$, Ha = 0.1, $\alpha = \gamma = N_b = 0.3$, Sc = Pr = 1.0

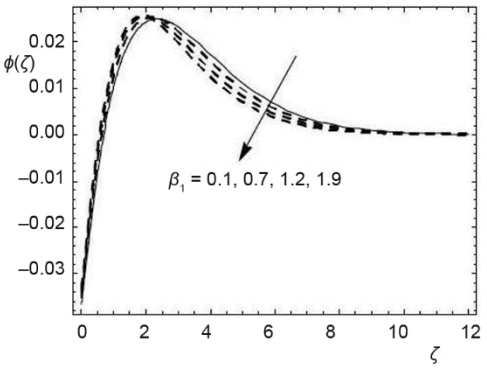

Figure 10. Curves of β_1 contrasted with $\phi(\zeta)$; $\beta_2 = 0.5$, Ha = $N_t = 0.1$, $\alpha = \gamma = N_b = 0.3$, Sc = Pr = 1.0

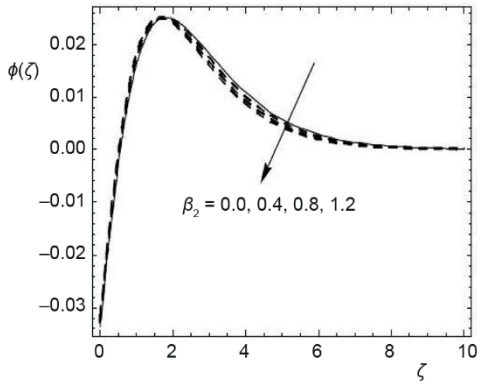

Figure 11. Curves of β_2 contrasted with $\phi(\zeta)$; β_1 = 0.5, Ha = N_t = 0.1, α = γ = N_b = 0.3, Sc = Pr = 1.0

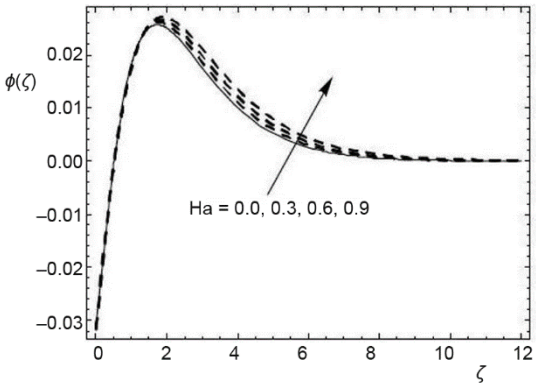

Figure 12. Curves of Hartman number contrasted with $\phi(\zeta)$; β_1 = β_2 = 0.5, N_t = 0.1, α = γ = N_b = 0.3, Sc = Pr = 1.0

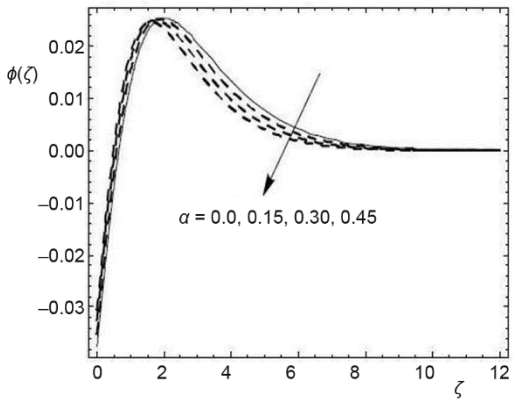

Figure 13. Curves of α contrasted with $\phi(\zeta)$; β_1 = β_2 = 0.5, Ha = N_t = 0.1, γ = N_b = 0.3, Sc = Pr = 1.0

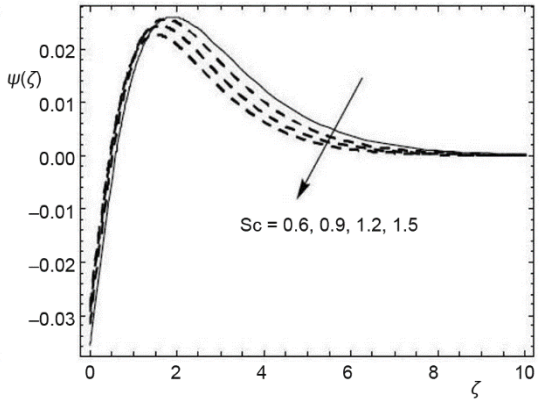

Figure 14. Curves of Schmidt number contrasted with $\phi(\zeta)$; β_1 = β_2 = 0.5, Ha = N_t = 0.1, α = γ = N_b = 0.3, Pr = 1.0

expanded concentration dispersion diminishes because of which concentration shows a diminishing pattern. Brownian boundary, N_b, when expanded, causes an adjustment in Brownian movement, which decreases the circulation of concentration as delineated via fig. 15. Expanding N_t leads increment in warm conduction of framework which gives in increment of concentration as observed *via* fig. 16. Figure 17 is conspired for the consequence of proportion boundary α on concentration rate, $r(\zeta)$. Here, $r(\zeta)$ is more *via* α. Figure 18 displays that bigger Sc_b compare to more $r(\zeta)$. Figure 19 depicts that bigger homogeneous-response boundary k_1 shows the decay in $r(\zeta)$. Figure 20 displays that increasing estimations of heterogeneous-response boundary k_2 comprises more $r(\zeta)$. Figure 21 displays the behavior of Hartman number and β_1 on $C_{\mathrm{f}}\mathrm{Re}_x^{1/2}$. Here $C_{\mathrm{f}}\mathrm{Re}_x^{1/2}$ enhances for Hartman number. Figure 22 depicts the impacts of α and β_1 on $C_{\mathrm{f}}\mathrm{Re}_x^{1/2}$. Here $C_{\mathrm{f}}\mathrm{Re}_x^{1/2}$ shows expanding conduct for the α and β_1. Figure 23 displays the features of Hartman number and β_1 on the $C_{\mathrm{g}}\mathrm{Re}_x^{1/2}$. Bigger Hartman number produces expanding function for $C_{\mathrm{g}}\mathrm{Re}_x^{1/2}$. Figure 24 reveals the influences of α and β_1 on $C_{\mathrm{g}}\mathrm{Re}_y^{1/2}$. From this figure it has been obtained that $C_{\mathrm{g}}\mathrm{Re}_y^{1/2}$ is a high bulk of the α. Effects of N_b and N_t on the $\mathrm{Nu}_x\mathrm{Re}_x^{1/2}$ are revealed through fig. 25. Here $\mathrm{Nu}_x\mathrm{Re}_x^{1/2}$ decays for N_t while the constant trend is watched for the N_b.

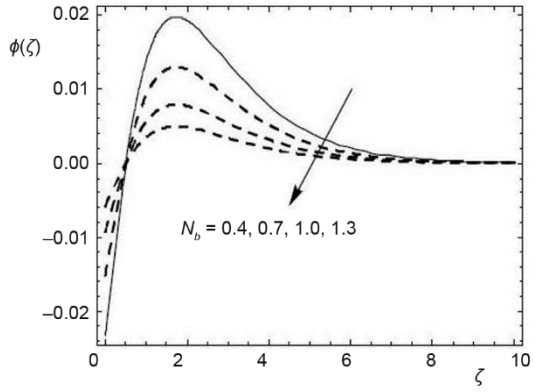

Figure 15. Curves of N_b contrasted with $\phi(\zeta)$; $\beta_1 = \beta_2 = 0.5$, Ha = $N_t = 0.1$, $\alpha = \gamma = 0.3$, Sc = Pr = 1.0

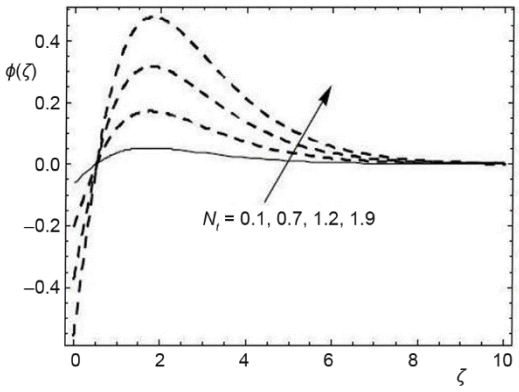

Figure 16. Curves of N_t contrasted with $\phi(\zeta)$; $\beta_1 = \beta_2 = 0.5$, Ha = 0.1, $\alpha = \gamma = N_b = 0.3$, Sc = Pr = 1.0

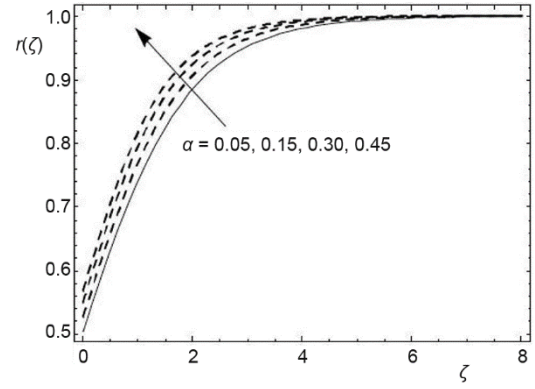

Figure 17. Curves of α contrasted with $r(\zeta)$; $\lambda = N_t = 0.2$, Fr = 0.1, $k_1 = \gamma = 0.3$, Sc = Pr = 1.0, N_b = Sc$_b$ = k_2 = 0.5

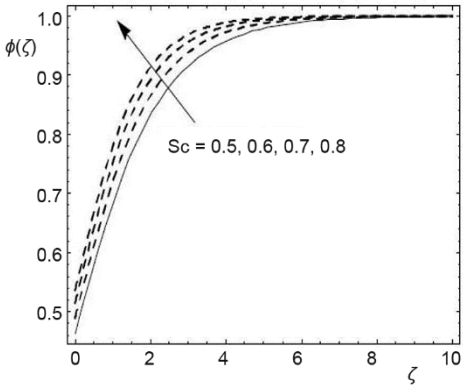

Figure 18. Curves of Schmidt number contrasted with $r(\zeta)$; $\alpha = \lambda = N_t = 0.2$, Fr = 0.1, $k_1 = \gamma = 0.3$, Pr = 1.0, N_b = Sc$_b$ = k_2 = 0.5

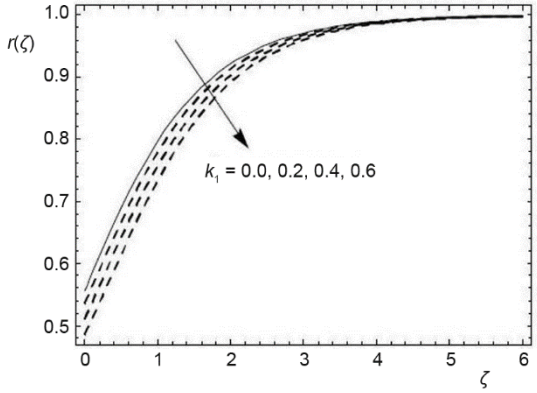

Figure 19. Curves of k_1 contrasted with $r(\zeta)$; $\alpha = \lambda = N_t = 0.2$, Fr = 0.1, $\gamma = 0.3$, Sc = Pr = 1.0, N_b = Sc$_b$ = k_2 = 0.5

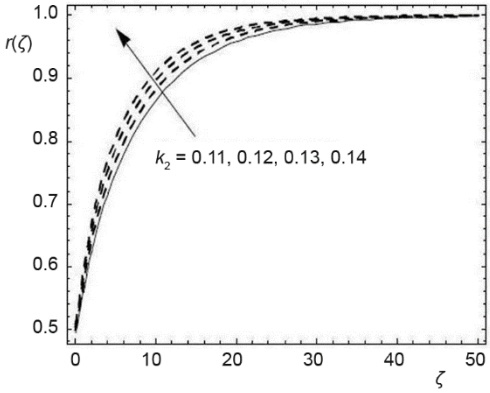

Figure 20. Curves of k_2 contrasted with $r(\zeta)$; $\beta_1 = \beta_2 = 0.5$, Ha = 0.1, $\alpha = \gamma = N_b = 0.3$, Sc = Pr = 1.0

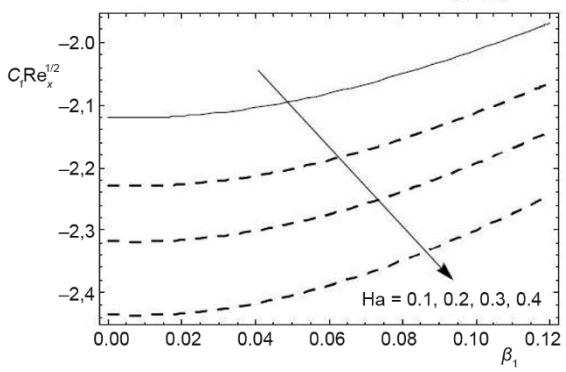

Figure 21. Curves of $C_f Re_x^{1/2}$ via Hartman number and β_1; β_2 = 0.5, N_t = 0.1, α = γ = N_b = 0.3, Sc = Pr = 1.0

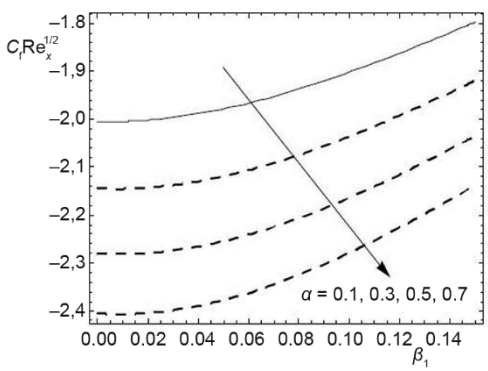

Figure 22. Curves of $C_f Re_x^{1/2}$ via α and β_1; β_2 = 0.5, Ha = N_t = 0.1, γ = N_b = 0.3, Sc = Pr = 1.0

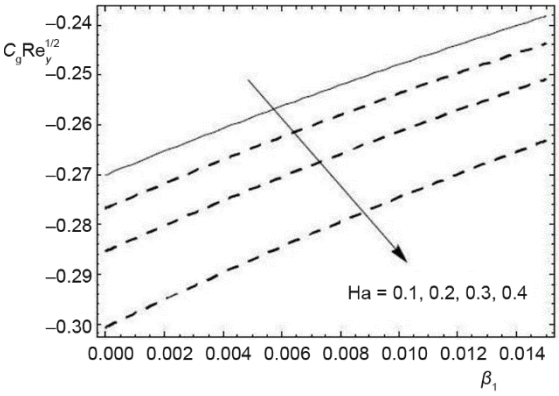

Figure 23. Curves of $C_g Re_x^{-1/2}$ via Hartman number and β_1; β_2 = 0.5, N_t = 0.1, α = γ = N_b = 0.3, Sc = Pr = 1.0

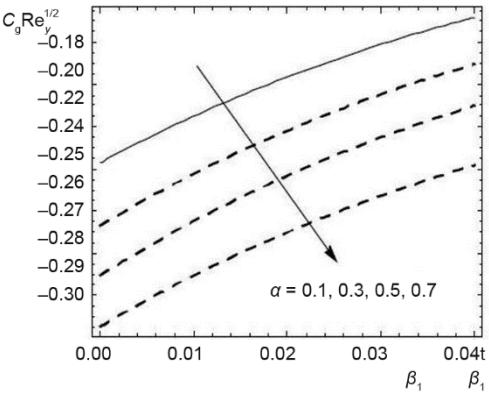

Figure 24. Curves of $C_g Re_x^{-1/2}$ via α and β_1; β_2 = 0.5, Ha = N_t = 0.1, γ = N_b = 0.3, Sc = Pr = 1.0

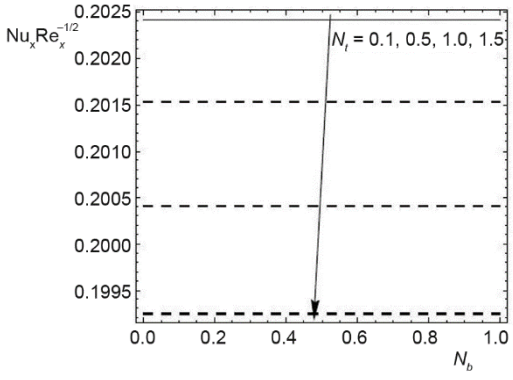

Figure 25. Curves of $Nu_x Re_x^{-1/2}$ via N_b and N_t; β_1 = β_2 = 0.5, Ha = 0.1, α = γ = 0.3, Sc = Pr = 1.0

Conclusions

Here the 3-D convective stream of magnetized Prandtl nanomaterial due to extendable sheet subject to heterogeneous-homogeneous responses is addressed. Random movement and thermophoretic features are accounted. Appropriate non-dimensional factors correspond to the non-linear ODE. Acquired non-linear differential frameworks are comprehended *via* the optimal homotopic procedure. The temperature, $\theta(\zeta)$, and the concentration, $\phi(\zeta)$, of nanomaterial present decay for the bigger Prandtl parameters, β_1 and β_2. An expansion in Hartman number depicts

more grounded $\theta(\zeta)$ and $\phi(\zeta)$. Bigger ratio parameter, α, delineates lower nanoparticles concentration, $\phi(\zeta)$, and the temperature, $\theta(\zeta)$, fields. Bigger, γ displays more grounded $\theta(\zeta)$. A similar trend is watched for different estimations of the N_t on the concentration $\phi(\zeta)$ and the temperature $\theta(\zeta)$ fields [38-43]. For bigger data of Prandtl number, temperature $\theta(\zeta)$ decays. Concentration rate $r(\zeta)$ is enhanced via Schmidt number Sc_b. An enhancement in k_1 leads to weaker concentration rate $r(\zeta)$ while the opposite trend is watched for k_2.

Acknowledgment

This project was funded by the Deanship of Scientific Research (DSR) at King Abdulaziz University, Jeddah, under grant no. G: 268-130-1441. The authors, therefore, acknowledge with thanks DSR for technical and financial support.

References

[1] Choi, S. U. S., Estman, J. A., Enhancing Thermal Conductivity of Fluids with Nanoparticles, *ASME International Mechanical Engineering Congress and Exposition*, San Francisco, Cal., USA, 1995
[2] Buongiorno, J., Convective Transport in Nanofluids, *Journal of Heat Transfer, 128* (2006), 3, pp. 240-250
[3] Jang, S. P., Choi, S. U. S., Role of Brownian Motion in the Enhanced Thermal Conductivity of Nanofluids, *Applied Physics Letters, 84* (2004), 21, pp. 4316-4318
[4] Bhattacharya, P., *et al*., Brownian Dynamics Simulation to Determine the Effective Thermal Conductivity of Nanofluids, *Journal of Applied Physics, 95* (2004), 11, pp. 6492-6494
[5] Tiwari, R. K., Das, M. K., Heat Transfer Augmentation in a Two-Sided Lid-Driven Differentially Heated Square Cavity Utilizing Nanofluid, *International Journal of Heat and Mass Transfer, 50* (2007), 9, pp. 2002-2018
[6] Kakac, S., Pramuanjaroenkij, A., Review of Convective Heat Transfer Enhancement with Nanofluids, *International Journal of Heat and Mass Transfer, 52* (2009), 13, pp. 3187-3196
[7] Abu-Nada, E., Oztop, H. F., Effects of Inclination Angle on Natural Convection in Enclosures Filled with Cu-Water Nanofluid, *International Journal of Heat and Fluid Flow, 30* (2009), 4, pp. 669-678
[8] Mustafa, M., *et al*., Stagnation-Point Flow of a Nanofluid Towards a Stretching Sheet, *International Journal of Heat and Mass Transfer, 54* (2011), 25, pp. 5588-5594
[9] Turkyilmazoglu, M., Exact Analytical Solutions for Heat and Mass Transfer of MHD Slip Flow in Nanofluids, *Chemical Engineering Science, 84* (2012), Dec., pp. 182-187
[10] Turkyilmazoglu, M., Pop, I., Heat and Mass Transfer of Unsteady Natural Convection Flow of Some Nanofluids Past a Vertical Infinite Flat Plate with Radiation Effect, *International Journal of Heat and Mass Transfer, 59* (2013), Apr., pp. 167-171
[11] Hsiao, K. L., Nanofluid Flow with Multimedia Physical Features for Conjugate Mixed Convection and Radiation, *Computers & Fluids, 104* (2014), Nov., pp. 1-8
[12] Hayat, T., *et al*., Magnetohydrodynamic Three-Dimensional Flow of Viscoelastic Nanofluid in the Presence of Nonlinear Thermal Radiation, *Journal of Magnetism and Magnetic Materials, 385* (2015), July, pp. 222-229
[13] Chamkha, A., *et al*., Non-Darcy Natural Convection Flow for Non-Newtonian Nanofluid Over Cone Saturated in Porous Medium with Uniform Heat and Volume Fraction Fluxes, *International Journal of Numerical Methods for Heat & flow, 25* (2015), 2, pp. 422-437
[14] Ellahi, R., *et al*., Shape Effects of Nanosize Particles in Cu-H_2O Nanofluid on Entropy Generation, *International Journal of Heat and Mass Transfer, 81* (2015), Feb., pp. 449-456
[15] Lin, Y., *et al*., MHD Pseudo-Plastic Nanofluid Unsteady Flow and Heat Transfer in a Finite Thin Film Over Stretching Surface with Internal Heat Generation, *International Journal of Heat and Mass Transfer, 84* (2015), May, pp. 903-911
[16] Merkin, J. H., A Model for Isothermal Homogeneous-Heterogeneous Reactions in Boundary Layer Flow, *Mathematical and Computer Modelling, 24* (1996), 8, pp. 125-136
[17] Chaudhary, M. A., Merkin, J. H., A Simple Isothermal Model for Homogeneous-Heterogeneous Reactions in Boundary-Layer Flow, II Dfferent Diffusivities for Reactant and Autocatalyst, *Fluid Dynamics Research, 16* (1995), 6, pp. 335-359
[18] Kameswaran, P. K., *et al*., Homogeneous-Heterogeneous Reactions in a Nanofluid Flow Due to Porous Stretching Sheet, *International Journal of Heat and Mass Transfer, 57* (2013), 2, pp. 465-472

[19] Imtiaz, M., *et al*., Homogeneous-Heterogeneous Reactions in MHD Flow Due to an Unsteady Curved Stretching Surface, *Journal of Molecular Liquids, 221* (2016), Sept., pp. 245-253
[20] Sajid, M., *et al*., Effect Of Homogeneous-Heterogeneous Reactions and Magnetohydrodynamics on Fe_3O_4 Nanofluid for the Blasius Flow with Thermal Radiations, *Journal of Molecular Liquids, 233* (2017), May, pp. 115-121
[21] Hayat, T., *et al*., Three-Dimensional Flow with Cattaneo-Christov Double Diffusion and Homogeneous-Heterogeneous Reactions, *Results in Physics, 7* (2017), Aug., pp. 2812-2820
[22] Khan, M. I., *et al*., Numerical Analysis for Darcy-Forchheimer Flow in Presence of Homogeneous-Heterogeneous Reactions, *Results in Physics, 7* (2017), July, pp. 2644-2650
[23] Hayat, T., *et al*., Influences of Hall Current and Chemical Reaction in Mixed Convective Peristaltic Flow of Prandtl Fluid, *Journal of Magnetism and Magnetic Materials, 407* (2016), June, pp. 321-327
[24] Soomro, F. A., *et al*., Passive Control of Nanoparticle Due to Convective Heat Transfer of Prandtl Fluid Model at the Stretching Surface, *Chinese Journal of Physics, 55* (2017), 4, pp. 1561-1568
[25] Kumar, K. G., *et al*., Effects of Mass Transfer on MHD Three Dimensional Flow of a Prandtl Liquid Over a Flat Plate in the Presence of Chemical Reaction, *Results in Physics, 7* (2017), Sept., pp. 3465-3471
[26] Hayat, T., *et al*., Three-Dimensional Flow of Prandtl Fluid with Cattaneo-Christov Double Diffusion, *Results in Physics, 9* (2018), Mar., pp. 290-296
[27] Makinde, O. D., Aziz, A., Boundary Layer Flow of a Nanofluid Past a Stretching Sheet with a Convective Boundary Condition, *International Journal of Thermal Sciences, 50* (2011), 7, pp. 1326-1332
[28] Hayat, T., *et al*., A Revised Model for Stretched Flow of Third Grade Fluid Subject to Magneto Nanoparticles and Convective Condition, *Journal of Molecular Liquids, 230* (2017), Mar., pp. 608-615
[29] Kuznetsov, A. V., Nield, D. A., Natural Convective Boundary-Layer Flow of a Nanofluid Past a Vertical Plate: A Revised Model, *International Journal of Thermal Sciences, 77* (2014), Mar., pp. 126-129
[30] Hayat, T., *et al*., A Revised Model for Jeffrey Nanofluid Subject to Convective Condition and Heat Generation/Absorption, *Plos One, 12* (2017), Feb., pp. 1-22
[31] Liao, S. J., An Optimal Homotopy-Analysis Approach for Strongly Nonlinear Differential Equations, Commun, *Communications in Nonlinear Science and Numerical Simulation, 15* (2010), 8, pp. 2003-2016
[32] Dehghan, M., *et al*., Solving Nonlinear Fractional Partial Differential Equations Using the Homotopy Analysis Method, *Numerical Methods for Partial Differential Equations, 26* (2010), 2, pp. 448-479
[33] Abd Elmaboud, Y., *et al*., Series Solution of a Natural Convection Flow for a Carreau Fluid in a Vertical Channel With Peristalsis, *Journal of Hydrodynamics, Ser. B, 27* (2015), 6, pp. 969-979
[34] Hayat, T., *et al*., Effects of Homogeneous and Heterogeneous Reactions in Flow of Nanofluids Over a Nonlinear Stretching Surface with Variable Surface Thickness, *Journal of Molecular Liquids, 221* (2016), Sept., pp. 1121-1127
[35] Hayat, T., *et al*., Darcy-Forchheimer Three-Dimensional Flow of Williamson Nanofluid Over a Convectively Heated Nonlinear Stretching Surface, *Communications in Theoretical Physics, 68* (2017), 3, pp. 387-394
[36] Muhammad, T., *et al*., A Revised Model for Darcy-Forchheimer Flow of Maxwell Nanofluid Subject to Convective Boundary Condition, *Chinese Journal of Physics, 55* (2017), 3, pp. 963-976
[37] Saif, R. S., *et al*., Stagnation-Point Flow of Second Grade Nanofluid Towards a Nonlinear Stretching Surface with Variable Thickness, *Results in Physics, 7* (2017), Aug., pp. 2821-2830
[38] Wakif, A., *et al*., Thermal Radiation and Surface Roughness Effects on the Thermo-Magneto-Hydrodynamic Stability of Alumina-Copper Oxide Hybrid Nanofluids Utilizing the Generalized Buongiorno's Nanofluid Model, *Journal of Thermal Analysis and Calorimetry, 143* (2020), 2, pp. 1201-1220
[39] Rasool, G., Wakif, A., Numerical Spectral Examination of EMHD Mixed Convective Flow of Second-Grade Nanofluid Towards a Vertical Riga Plate Using an Advanced Version of the Revised Buongiorno's Nanofluid Model, *Journal of Thermal Analysis and Calorimetry, 143* (2020), 3, pp. 2379-2393
[40] Zaydan, M., *et al*., Significances of Blowing and Suction Processes on the Occurrence of Thermo-Magneto-Convection Phenomenon in a Narrow Nanofluidic Medium: A Revised Buongiorno's Nanofluid Model, *Case Studies in Thermal Engineering, 22* (2020), Dec., ID 100726
[41] Shah, N. A., *et al*., Significance of Suction and Dual Stretching on the Dynamics of Various Hybrid Nanofluids: Comparative Analysis Between Type I and Type II Models, *Physica Scripta, 95* (2020), 9, ID 095205

[42] Usman, L. P., *et al*., Similarity Solution of the Partial Differential Equations that Model Water/Magnetite Nanofluid Flow and Heat Transfer on a Stretchable Rotating Disk Subject to Thermal Radiation and Lorentz Force, *Numerical Methods for Partial Differential Equations*, On-line first, https://doi.org/10.1002/num.22677, 2020
[43] Ahmad, S., *et al*., Dual Nature Solutions for Temperature-Dependent Transport Properties of Nanofluid Flow with Entropy Generation, *Numerical Methods for Partial Differential Equations*, On-line first, https://doi.org/10.1002/num.22679, 2020

Paper submitted: July 8, 2021
Paper revised: July 15, 2021
Paper accepted: July 28, 2021